PCCP

Accepted Manuscript

ROYAL SOCIETY OF CHEMISTRY

www.rsc.org/pccp

Submitted to Phys. Chem. Chem. Phys.

Formation of C_3H_2, C_5H_2, C_7H_2, and C_9H_2 from Reactions of CH, C_3H, C_5H, and C_7H Radicals with C_2H_2

Yi-Lun Sun, Wen-Jian Huang, and Shih-Huang Lee*

National Synchrotron Radiation Research Center (NSRRC), 101 Hsin-Ann Road, Hsinchu Science Park, Hsinchu 30076, Taiwan

*Author to whom correspondence should be addressed. Tel: +886-3-578-0281.

Fax: +886-3-578-3813. Electronic mail: shlee@nsrrc.org.tw

Abstract

The $C_{m+2}H_2$ family can be classified into two categories – $C_{2n+1}H_2$ and $C_{2n+2}H_2$. $C_{m+2}H_2$ are proposed to be important intermediates in syntheses of large carbonaceous molecules. The understanding on the formation mechanisms of both odd and even carbon-numbered $C_{m+2}H_2$ is beneficial to the atmospheric, astronomical, and combustion chemistry. $HC_{2n+2}H$ (polyynes) are believed to be producible from the $C_{2n}H + C_2H_2$ and $C_2H + C_{2n}H_2$ reactions but $C_{2n+1}H_2$ ($n \geq 2$) attract less attention on their formation mechanisms. In the present work, we make up the lack of knowledge on the $C_{2n+1}H_2$ formation mechanisms by investigating the reactions $C_{2n-1}H + C_2H_2 \rightarrow C_{2n+1}H_2 + H$ with n = 1 – 4. The dynamics of reactions of $C_{2n-1}H$ radicals with C_2H_2 are explored in crossed molecular beams by interrogating products $C_{2n+1}H_2$. Products' translational-energy and angular distributions of the hydrogen-loss channels are unraveled by measuring time-of-flight spectra and photoionization-efficiency spectra of $C_{2n+1}H_2$ with tunable synchrotron vacuum-ultraviolet ionization. The $C_{2n+1}H_2$ product includes two isomers *c*-$^1HC_{2n-1}(C)CH$ and $^3HC_{2n+1}H$ identified by the maximal translational-energy release and the photoionization threshold. Furthermore, the quantum-chemical calculations indicate that the title reactions incur a small or negligible entrance barrier and are nearly isoergic except the barrierless exothermic reaction $CH + C_2H_2 \rightarrow C_3H_2 + H$. It is the first time to demonstrate that C_5H_2, C_7H_2, and C_9H_2 are producible from the title reactions. In conjunction with the studies on the $C_{2n}H + C_2H_2$ reactions, a brief picture for the C_mH (m = 1 – 8) + $C_2H_2 \rightarrow C_{m+2}H_2 + H$ reactions can be outlined.

I. Introduction

$C_{2n}H$ (n = 1 – 4) were detected in the line of sight toward the Taurus Molecular Cloud (TMC-1)[1,2,3,4] and the circumstellar envelope of carbon star IRC+10216.[5] In contrast, the $C_{2n}H$ radicals were not detected yet in flames due to their high reactivities and low concentrations. Nonetheless, the type-1 reaction $C_{2n}H + C_2H_2 \rightarrow C_{2n+2}H_2 + H$ is suggested to be a major source for formation of polyynes ($HC_{2n+2}H$) that have been found in the atmosphere of Titan,[6] the moon of Saturn, the circumstellar envelope of protoplanetary nebula CRL 618,[7] and hydrocarbon flames.[8] Polyynes are proposed to be important intermediates for syntheses of large carbonaceous molecules such as polycyclic aromatic hydrocarbons (PAHs), fullerenes, and soot.

$C_{2n}H + C_2H_2 \rightarrow C_{2n+2}H_2 + H$ (1)

Of all the reactions (1), however, only the reactions of C_2H and C_4H radicals with ethyne (C_2H_2) were investigated. The rate coefficient of the C_2H (C_4H) + C_2H_2 reaction was determined as 1.06×10^{-10} – 2.27×10^{-10} (1.54×10^{-10} – 3.90×10^{-10}) cm^3 $molecule^{-1}$ s^{-1} in the temperature range 15 – 295 (39 – 300) K with a maximum at 15 (52) K.[9,10,11,12] The dynamics of reactions C_2D + $C_2H_2 \rightarrow C_4HD + H$ / $C_4D + H_2$ with a branching ratio of 98–99% / 1–2% were explored in crossed molecular beams using product translational spectroscopy and quantum-chemical calculations.[13] The H-loss channel was exothermic whereas the H_2-loss channel was endothermic but energetically accessible at collision energy (E_c) 6.2 kcal mol^{-1}. The H-loss channel favored the sideway direction whereas the H_2-loss channel preferred the forward and backward directions in angular distributions. Recently, the dynamics of reactions of $C_{2n}H$ (n = 1 – 4) with C_2H_2 at E_c = 9.9, 13.1, 14.8, and 15.9 kcal mol^{-1}, respectively, were explored using a crossed molecular-beam apparatus and synchrotron vacuum-ultraviolet (VUV) ionization.[14] The $C_{2n+2}H_2$ products of the H-loss channels were identified as polyynes exclusively with the product translational and photoionization spectroscopies.[14]

Ethyne is well known as an abundant interstellar species and an important combustion intermediate. The existence of $C_{2n-1}H$ radicals in CRL 618,[15] TMC-1,[3,4,16,17] and IRC+10216[5]

gives an implication for the formation of $C_{2n+1}H_2$ from the type-2 reaction $C_{2n-1}H + C_2H_2 \rightarrow C_{2n+1}H_2 + H$. Up to date, however, only linear (hereafter denoted as *l*-) and cyclic (hereafter denoted as *c*-) C_3H_2 in the $C_{2n+1}H_2$ family were detected in interstellar space.[3,5,15] $C_{2n-1}H$ and $C_{2n+1}H_2$ are open-shell and potentially reactive molecules so that their concentrations are commonly not high enough to detect in flames. Nonetheless, C_3H_2 could be detected in fuel-rich flames of several hydrocarbons like ethyne,[18] ethene,[19] propene,[20] and cyclopentene.[21] C_3H_2 was identified to be a mixture of several isomers (e.g., *c*-C_3H_2, HCCCH, and H_2CCC) by the VUV photoionization spectroscopy and simulation. C_5H_2 was also claimed to be detected in the cyclopentene flame[22] but no experimental result was reported due to its low concentration. In contrast to the type-1 reactions, the type-2 reactions attract less attention in most chemical models but the CH + C_2H_2 reaction.

$C_{2n-1}H + C_2H_2 \rightarrow C_{2n+1}H_2 + H$ (2)

To our knowledge, there is no literature report for the reactions (2) but for the CH + $C_2H_2 \rightarrow C_3H_2 + H$ reaction. The rate coefficient of the CH + C_2H_2 reaction was determined as $(3.85–4.83)\times10^{-10}$ cm^3 $molecule^{-1}$ s^{-1} in the temperature range 23–295 K with a maximum at 75 K.[23] The rate coefficient was also determined as $(2.2\pm0.4)\times10^{-10}$, $(4.2\pm0.4)\times10^{-10}$, $(3.2\pm0.2)\times10^{-10}$, and $(3.6\pm0.6)\times10^{-10}$ cm^3 $molecule^{-1}$ s^{-1} at 298 or 300 K.[24,25,26,27] The H-atom branching ratio in the CH + C_2H_2 reaction was determined as 0.90 ± 0.08 [27] and 1.05 ± 0.09 [28] using laser-induced fluorescence at 121.6 nm, indicating that atomic hydrogen elimination is the dominant exit channel. The dynamics of reactions CH + C_2H_2, CH + C_2D_2, and CD + C_2H_2 were investigated in crossed molecular beams by measuring translational spectra of products C_3H_2, C_3H, and their deuterated analogues upon atomic and molecular hydrogen elimination.[29,30] The translational-energy distributions and the angular distributions of atomic and molecular hydrogen elimination channels were derived from the simulations of product translational spectra. The branching ratio of atomic to molecular hydrogen channel was determined as 91:9, 87:13, and 81:19 for the reactions CH +

C_2H_2, CH + C_2D_2, and CD + C_2H_2, respectively, at collision energy 4.0 kcal mol^{-1} in crossed beams[29,30] and as 85:15 for the CH + C_2H_2 reaction in a low-pressure C_2H_2/O_2 flame at 600 K.[31] The ratio of *c*-C_3H_2 to HCCCH/H_2CCC was determined as 35:65 in crossed molecular beams by simulating C_3H_2 translational spectra[29] but as 90^+:10^- in a flow reactor coupled to a photoionization mass spectrometer by simulating C_3H_2 photoionization spectra.[32] The large branching to *c*-C_3H_2 in a flow reactor was attributed to a fast H-assisted isomerization mechanism of HCCCH into *c*-C_3H_2.[32]

Quantum-chemical calculations indicated that the reaction CH + C_2H_2 → *l*-/*c*-C_3H_3 → *l*-/*c*-C_3H_2 + H was exothermic and had no entrance barrier,[32,33,34,35,36] in accord with the kinetics measurements.[23] The potential-energy-surface calculations indicated that CH can add to C_2H_2 to form a complex H_2CCCH, *c*-HC(CH)CH, or HCCHCH at entrance channels. Isomerization of the intermediates can take place before decomposition to *c*-C_3H_2/HCCCH/H_2CCC + H and C_3H + H_2. The product branching ratios were calculated with Rice-Ramsperger-Kassel-Marcus (RRKM) theory based on the potential-energy surfaces established at various theoretical levels.[32,33,34,35,36] Most of the RRKM calculations[32,35,36] predicted that the product HCCCH + H is dominant, *c*-C_3H_2 + H is medium, and H_2CCC + H and C_3H + H_2 are merely minor.

The absence of knowledge on the dynamics of reactions (2) with $n \geq 2$ drives us to investigate the title reactions. Angle-specific time-of-flight (TOF) spectra and photoionization-efficiency (PIE) spectra of products $C_{2n+1}H_2$ were measured using the crossed-molecular-beam quadrupole-mass apparatus and the synchrotron VUV photoionization. Furthermore, the potential-energy surfaces of the title reactions were established with quantum-chemical calculations.

II. Experiments

The experiments were conducted in a crossed-molecular-beam quadrupole-mass apparatus[37] using synchrotron VUV light as the ionization source. One source chamber was equipped with an

Even-Lavie valve and a two-electrode discharge device[38] to produce $C_{2n-1}H$ radicals from a mixture of 1% C_2H_2 seeded in He. A gas pulse was expanded through the discharge device with a stagnation pressure of 7.2×10^5 Pa. Meanwhile, a high-voltage pulse (-1 kV, 10 μs) was applied to the discharge cathode to ignite a plasma along with production of a variety of hydrocarbon species of which $C_{2n-1}H$ (n = 1 – 4) served as the reactants in the present work. The radical beam collimated with two successive skimmers had a most-probable speed 1850 – 1870 m s^{-1}, depending slightly on the $C_{2n-1}H$ radicals, and had a speed ratio (V/ΔV) larger than 7. The other source chamber was equipped also with an Even-Lavie valve to expand a mixture of 5% C_2H_2/He at a stagnation pressure of 7.2×10^5 Pa. The molecular beam collimated with a skimmer had a most-probable speed 1725 m s^{-1} and a speed ratio larger than 7. Both the reactant beams intercepted at 90° in the reaction chamber under a single-collision condition with E_c = 6.7, 11.8, 14.1, and 15.4 kcal mol^{-1} for n = 1 – 4, respectively. After reactive collisions, the products scattered into a small solid angle were ionized with synchrotron VUV radiation that had a beam size of diameter ~ 1 mm, a photon flux ~ 8×10^{15} photons s^{-1}, and an energy resolution (ΔE/E) ~ 4.2%. A quadrupole-mass filter served to select the desired product cations with a specific mass-to-charge ratio (m/z). The selected products were detected with a Daly-type ion counter. A multichannel scaler (MCS) sampled the ion signals into 4000 bins of width 1 μs. After subtraction of the ion flight interval from the total flight duration, a neutral product TOF spectrum was obtained. The two Even-Lavie valves, the discharge device, and the MCS were synchronized at optimal timing with two pulse generators operating at 200 Hz. The source-chamber assembly was rotatable, which enabled measurements of products' laboratory angular distributions. Product TOF spectra were recorded with a fixed photon energy by scanning the laboratory angle (Θ) back to back in a pertinent angular range. Θ was defined as the angle between the detection axis and the radical beam; Θ = 0° (90°) was the incidence angle of $C_{2n-1}H$ (C_2H_2). In the measurement of photoionization spectra, product TOF spectra were recorded at a fixed laboratory angle by tuning

the VUV photon energy back to back in the range 7.6 – 11.6 eV. All the TOF spectra recorded at the same experimental condition were summed together to yield a satisfactory signal-to-noise ratio and to avoid a long-term drift.

III. Calculations

The quantum-chemical calculations were carried out with a suite of programs Gausian-03 in a computer equipped with a six-core processor and 64 GB of memory. Molecular structures and zero-point energies (ZPEs) were calculated with a density-functional method B3LYP and a basis set aug-cc-pVDZ. An optimized molecular species was judged as a stationary or transition structure by its imaginary vibrational-frequency number. The connection of a transition structure with its reactant and product were confirmed with the calculation of intrinsic reaction coordinate (IRC). The absence of a transition state on a reaction path was justified with the calculation of potential-energy-surface scan. Both the IRC and SCAN calculations were performed at the level of B3LYP/aug-cc-pVDZ. Based on the optimized structure, the total energy of a molecular species was calculated with a couple-cluster method CCSD(T) and a basis set aug-cc-pVTZ. Besides, the structure, ZPE, and total energy of a molecular cation were calculated with the same computational method as for a neutral species. The adiabatic ionization energy of a molecular species (e.g., reactant and product) was calculated by the cationic-neutral energy difference corrected with ZPEs. As the desired cationic structure cannot be optimized, e.g., the singlet cyclic cationic structure of cyclic reactants *c*-HC(C)C, *c*-HC_3(C)C, and *c*-HC_5(C)C, we calculated the vertical ionization energy using the neutral equilibrium structure as the cationic structure.

IV. Results and analysis

The reactants $C_{2n-1}H$ (n = 1 – 4) were synthesized from 1% C_2H_2/He by pulsed high-voltage discharge. The discharge current and width were set at 20 mA and 10 μs to optimize the temporal resolution and the intensity of crossed-beam reaction products. In order to estimate the relative

concentrations of discharge products, we measured the mass distribution of discharge products as presented in the supporting information of Ref. 14. The mass spectrum indicated that the discharge products containing more than three hydrogen atoms and the discharge products having a mass larger than 100 u are scarce.[14] Note that the yields of discharge products depend on the performances of the Even-Lavie valve and the discharge device. It is necessary to monitor the discharge stability and to characterize the discharge molecular beam.

Figure 1 presents the PIE spectra of reactants C_3H, C_5H, and C_7H synthesized in the radical beam. Each $C_{2n-1}H$ (n = 2 – 4) species has a linear isomer *l*-$C_{2n-1}H$ and a three-member-ring isomer *c*-$HC_{2n-3}(C)C$. *c*-HC(C)C is 1.4 kcal mol^{-1} more stable than *l*-C_3H. In contrast, *c*-$HC_3(C)C$ is 2.9 kcal mol^{-1} less stable than *l*-C_5H and *c*-$HC_5(C)C$ is 2.7 kcal mol^{-1} less stable than *l*-C_7H. The adiabatic ionization energies of *l*-$C_{2n-1}H$ to the singlet linear cationic state were calculated to be 9.01, 8.29, and 7.79 eV for n = 2 – 4. Because the singlet cyclic cationic structure cannot be optimized, the vertical ionization energies of *c*-$HC_{2n-3}(C)C$ to the singlet state were calculated as 9.91, 9.27, and 7.86 eV for n = 2 – 4. Furthermore, the ionization energies of *c*-$HC_{2n-3}(C)C$ to the triplet cyclic cationic state were calculated as 10.05, 9.71, and 9.46 eV that are higher than the vertical ionization energy to the singlet state. Therefore, the vertical ionization to the singlet cationic state is assigned to the ionization energy of *c*-$HC_{2n-3}(C)C$. Upon assumption of thermal equilibrium at 1000 K, the concentration ratio is estimated as 1.01 for *c*-HC(C)C to *l*-C_3H, 0.12 for *c*-$HC_3(C)C$ to *l*-C_5H, and 0.13 for *c*-$HC_5(C)C$ to *l*-C_7H with the aforementioned enthalpy differences and with a degeneracy ratio of 1:2 for the cyclic to linear isomer. The PIE spectra of C_3H and C_5H produced from the reactions $^3C + C_2H_2 \rightarrow$ *l*-/*c*-$C_3H + H$ and $^3C_3 + C_2H_2 \rightarrow$ *l*-$C_5H + H$ [39] in crossed molecular beams are also presented in Fig. 1 for comparison. Apparently, the C_3H reactant includes both linear and cyclic isomers but the C_5H reactant is dominated by its linear isomer.

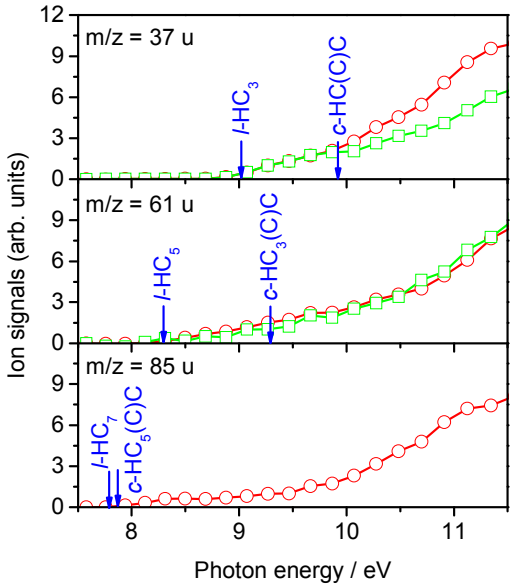

Figure 1. PIE spectra of reactants C_3H (m/z = 37 u), C_5H (m/z = 61 u), and C_7H (m/z = 85 u). Red circles represent the spectra of C_3H, C_5H, and C_7H produced from 1% C_2H_2/He by discharge. Green squares represent the spectra of C_3H and C_5H produced from the reactions $^3C + C_2H_2 \rightarrow$ *l*-/*c*-$C_3H + H$ and $^3C_3 + C_2H_2 \rightarrow$ *l*-$C_5H + H$ in crossed molecular beams. Each baseline was shifted to zero. The variation of photon flux versus photon energy was not corrected. Arrows indicate the calculated ionization energies of isomers *l*-$C_{2n-1}H$ and *c*-$HC_{2n-3}(C)C$.

Figure 2 depicts four Newton diagrams for the $C_{2n-1}H$ (n = 1 – 4) + C_2H_2 reactions that have reactant collision energies 6.7, 11.8, 14.1, and 15.4 kcal mol^{-1}, respectively. V_{C2n-1H} (V_{C2H2}) denotes the velocity 1870 (1725) m s^{-1} of reactant $C_{2n-1}H$ (C_2H_2) with a direction at the laboratory angle $\Theta = 0°$ (90°). Each reaction system has a center of mass (CM) traveling along Θ_{CM} that is 61.5°, 33.0°, 21.5°, and 15.8° for n = 1 – 4, respectively. The horizontal line of each Newton diagram denotes the relative velocity V_{rel} = 2544 m s^{-1} between $C_{2n-1}H$ and C_2H_2. Each diagram is superimposed with the two-dimensional velocity-distribution contour of product $C_{2n+1}H_2$. Because

the $C_{2n+1}H_2$ product has a small velocity in the CM frame due to atomic hydrogen elimination, the product is concentrated near Θ_{CM}. Dashed lines denote the detection axes at several laboratory angles. The TOF spectra of products C_3H_2 (m/z = 38 u), C_5H_2 (m/z = 62 u), C_7H_2 (m/z = 86 u), and C_9H_2 (m/z = 110 u) were recorded at 16 – 22 laboratory angles with photon energy 11.6 eV except for the C_7H_2 product that was ionized with photons at 10.3 eV in order to avoid interference of impurities in the C_2H_2/He mixtures.

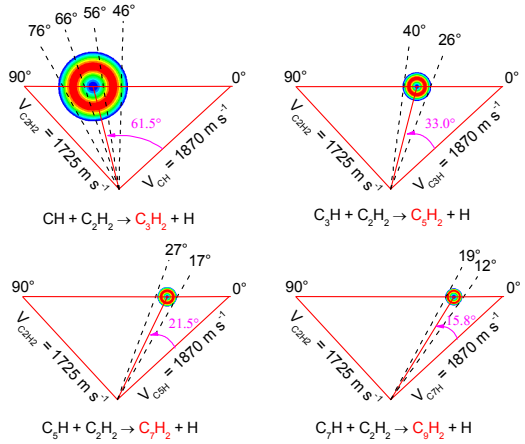

Figure 2. Newton diagrams superimposed with the product velocity-distribution maps for the reactions $C_{2n-1}H$ (n = 1 – 4) + C_2H_2. V_{C2n-1H} and V_{C2H2} denote the velocities of $C_{2n-1}H$ and C_2H_2. Θ_{CM} equals 61.5°, 33.0°, 21.5°, and 15.8° for n = 1 – 4. Dashed lines denote the detection axes at several laboratory angles.

In addition to the reaction $^{12}C_{2n-1}H + {}^{12}C_2H_2 \rightarrow {}^{12}C_{2n+1}H_2 + H$, the isotopic reaction $^{13}C^{12}C_{2n-2} + {}^{12}C_2H_2$ (or $^{12}C_{2n-1} + {}^{13}C^{12}CH_2$) $\rightarrow {}^{13}C^{12}C_{2n}H + H$ has a small contribution to the ion signals recorded at m/z = 12×(2n+1)+2. The ion signals at m/z = 37, 61, 85, and 109 u are 3.1, 0.1, 0.4, and 0.5 times the ion signals at m/z = 38, 62, 86, and 110 u recorded at 63°, 34°, 22°, and 16°, respectively, with photon energy 11.6 eV. Considering the natural isotopic ratio 0.011 of ^{13}C to ^{12}C,

the contribution of $^{13}C^{12}C_2H$ to m/z = 38 u has a ratio of ~ 0.011×3×3.1 = 0.10. In the same manner, the ratios are evaluated as 0.006, 0.03, and 0.05 for the contributions of $^{13}C^{12}C_4H$ to 62 u, $^{13}C^{12}C_6H$ to 86 u, and $^{13}C^{12}C_8H$ to 110 u, respectively. However, these ratios might be overestimated because the dissociative ionization $C_{2n+1}H_2 \rightarrow C_{2n+1}H^+ + H$ is ignored here. The ion signal recorded at m/z = 37 u was multiplied by a factor of 0.1, that was employed as the background $^{13}C^{12}C_2H$ to be subtracted from of the ion signal recorded at m/z = 38 u. Because the interference is ≤ 5% and the product ion signal is small in the other three reactions, the influence of $^{13}C^{12}C_{2n}H$ is neglected at m/z = 62, 86, and 110 u.

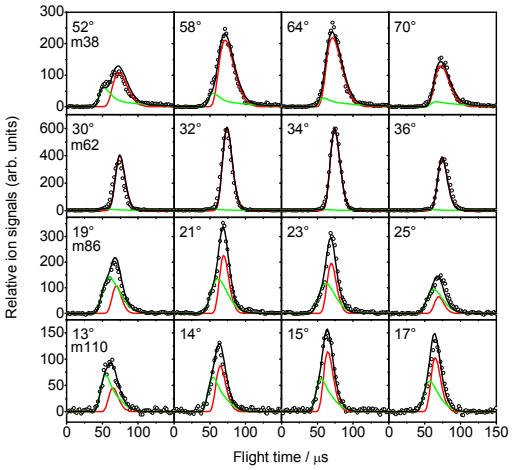

Figure 3. Angle-specific TOF spectra of products C_3H_2, C_5H_2, C_7H_2, and C_9H_2 recorded at m/z = 38, 62, 86, and 110 u, respectively. C_7H_2 was ionized with 10.3 eV whereas the other three species were ionized with 11.6 eV. Open circles denote the experimental data. Red and green curves represent the simulations of the reactive and nonreactive parts, respectively. Black curves are the sums of the red and green curves. Each panel shows the corresponding laboratory angle.

Figure 3 presents four selected TOF spectra and simulations for each product; here, data points were re-binned into a width of 2 μs to increase the signal-to-noise ratio. Each $C_{2n+1}H_2$ product has

two components arising separately from the $C_{2n-1}H + C_2H_2$ reaction (red line) and from the $C_{2n+1}H_2 + C_2H_2$ nonreactive scattering (green line); the $C_{2n+1}H_2$ species scattered by He has no contribution to the angular range interrogated. Figure 4 exhibits the corresponding laboratory angular distributions $P(\Theta)$ and the simulations for the reactive (red line) and nonreactive (green line) parts. The CM translational-energy distributions $P(E_t)$ employed to simulate the TOF spectra and the laboratory angular distributions of the title reactions are presented in Fig. 5. Here, E_t includes translational energies of both momentum-matched products $C_{2n+1}H_2$ and H. Arrows indicate the energetic limits of product isomers $^3HC_{2n+1}H + H$ and c-$^1HC_{2n-1}(C)CH + H$. The CM angular distribution $P(\theta)$ is nearly isotropic and thus omitted here. $\theta = 0°$ (180°) is defined as the incidence direction of $C_{2n-1}H$ (C_2H_2) in the CM frame. The $P(E_t)$ and $P(\theta)$ distributions were also employed to construct the product velocity-distribution maps shown in Fig. 2. The nonreactive part arising from the collision $C_{2n+1}H_2 + C_2H_2 \rightarrow C_{2n+1}H_2 + C_2H_2$ was simulated with a product translational-energy distribution biased to the energetic limit (i.e., the reactant collision energy) 11.9, 14.2, 15.4, and 16.3 kcal mol^{-1} for n = 1 – 4 and with a product angular distribution highly peaked at the forward direction. Because the nonreactive part is viewed as a background and not detected entirely in the laboratory angles, the employed translational-energy and angular distributions might not be accurate enough and thus are omitted here.

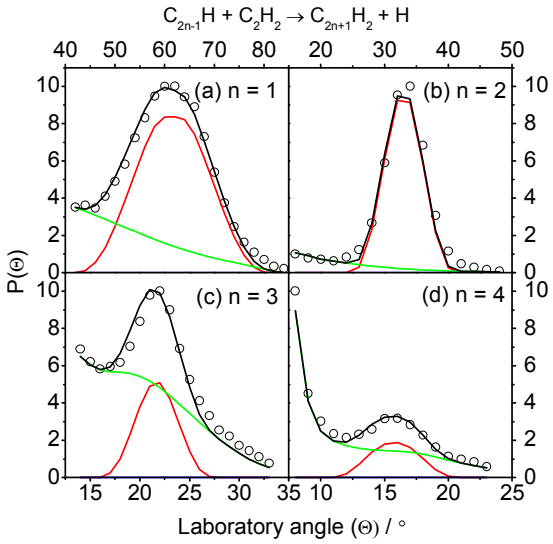

Figure 4. Laboratory angular distributions of products C_3H_2, C_5H_2, C_7H_2, and C_9H_2 recorded at m/z = 38, 62, 86, and 110 u, respectively. C_7H_2 was ionized with 10.3 eV whereas the other three species were ionized with 11.6 eV. Open circles denote the experimental data. Red and green curves represent the simulations of the reactive and nonreactive parts, respectively. Black curves are the sums of the red and green curves.

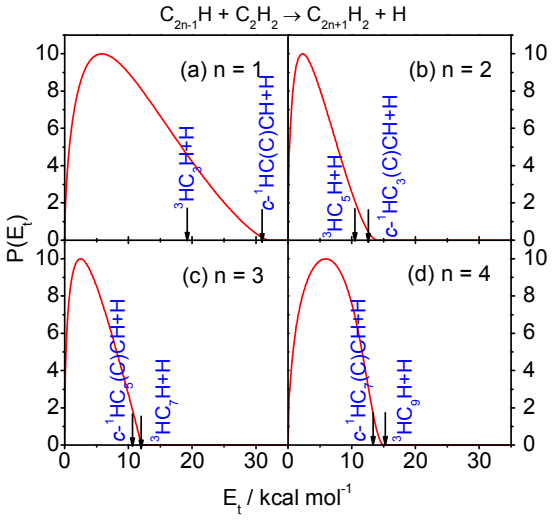

Figure 5. CM product translational-energy distributions for the reactions $C_{2n-1}H$ (n = 1 – 4) + C_2H_2 → $C_{2n+1}H_2$ + H. Arrows indicate the energetic limits of product isomers *c*-$^1HC_{2n-1}(C)CH$ + H and $^3HC_{2n+1}H$ + H.

Figure 6 exhibits the PIE spectra of products C_3H_2 (m/z = 38 u), C_5H_2 (m/z = 62 u), C_7H_2 (m/z = 86 u), and C_9H_2 (m/z = 110 u) recorded at Θ = 62°, 33°, 22° and 16°, respectively, in the energy range 7.6 – 11.6 eV. The ion signals were integrated in the TOF range of 30 – 110 μs. The part of $^{13}C^{12}C_2H$ at m/z = 38 u was subtracted as mentioned above. A background arising from the impurity in the C_2H_2/He mixture appeared at m/z = 86 u as the photon energy was above 10.3 eV. The background was obtained alone by switching off discharge and was subtracted from the ion signal recorded with discharge. The photon flux increases smoothly from 7.6 eV to 11.6 eV by a factor of ~ 10% based on the simulations of undulator radiation and mirror reflection. The variation was not corrected in the present experiments. The baseline of each PIE spectrum was shifted to zero. The dissociative ionization $C_{2n+x+1}H_{y+2} + h\nu \rightarrow C_{2n+1}H_2^+ + C_xH_y$ (x ≥ 1) + e^- was not observed in this photon-energy range. Arrows indicate the calculated adiabatic ionization energies of product isomers $^3HC_{2n+1}H$ and *c*-$^1HC_{2n-1}(C)CH$. Furthermore, the appearance of the product TOF spectrum appears to be insensitive to the photon energy, implying that both the reactive and nonreactive parts have similar PIE spectra. It is rationalized by the fact that the type-2 reaction is also responsible for the synthesis of $C_{2n+1}H_2$ (n = 1 – 4) in the C_2H_2 discharge.

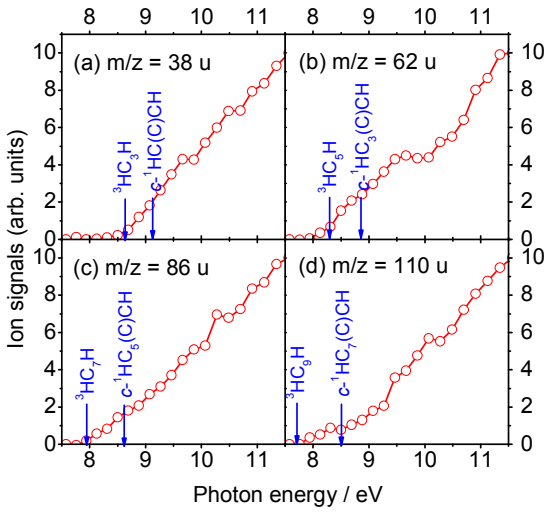

Figure 6. PIE spectra of products C_3H_2 (m/z = 38 u), C_5H_2 (m/z = 62 u), C_7H_2 (m/z = 86 u), and C_9H_2 (m/z = 110 u) recorded at Θ = 62°, 33°, 22°, and 16°, respectively. Each baseline was shifted to zero. The variation of photon flux versus photon energy was not corrected. Arrows indicate the calculated adiabatic ionization energies of *c*-$^1HC_{2n-1}(C)CH$ and $^3HC_{2n+1}H$.

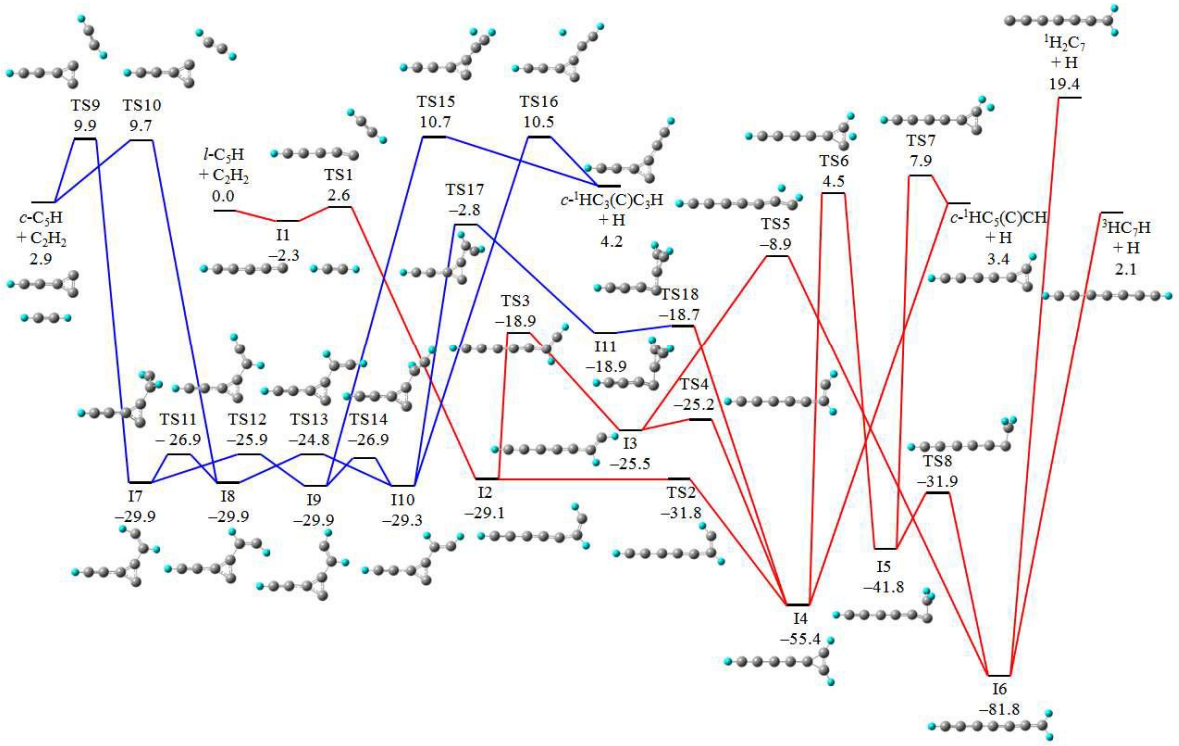

Figure 7. Potential-energy surface of the reaction $C_5H + C_2H_2 \rightarrow C_7H_2 + H$. The red (blue) line is for the linear (cyclic) C_5H reaction. The molecular structures are presented along with the corresponding potential-energy levels. The relative potential energies are given in kcal mol^{-1}.

Since the *ab-initio* potential-energy surface of the $CH + C_2H_2$ reaction has been reported in the literature,[32,33,34,35,36] the present calculations are focused on the reactions of two lowest-lying isomers *l*-$C_{2n-1}H$ and *c*-$HC_{2n-3}(C)C$ with C_2H_2 for n = 2 – 4. The potential-energy surfaces were

calculated with the method CCSD(T)/aug-cc-pVTZ//B3LYP/aug-cc-pVDZ including the correction of ZPEs at the level of B3LYP/aug-cc-pVDZ. Because the reactions of C_3H, C_5H, and C_7H with C_2H_2 have similar mechanisms, Fig. 7 presents the potential-energy surface and the molecular structures only for the $C_5H + C_2H_2$ reaction. The potential-energy surfaces and the molecular structures of the reactions of C_3H and C_7H with C_2H_2 were presented as Figure S1 and Figure S2, respectively, in the supplementary information. In each reaction, an intermediate is labeled with I# and a transition structure is labeled with TS#. For the $C_5H + C_2H_2$ reaction, TS2 lies above I2 at the B3LYP/aug-cc-pVDZ level but TS2 becomes below I2 at the level of CCSD(T)/aug-cc-pVTZ + ZPE, indicating that TS2 is negligible at the latter level of theory.

V. Discussion

The present calculations indicate that the terminal carbon atom of *l*-$C_{2n-1}H$ (n = 2 – 4) can add to a hydrogen atom of C_2H_2 to form a van-der-Waals (vdW) complex I1 that in turn rearranges to a meta-stable complex $HC_{2n-1}CHCH$ (I2) through a transition state TS1. TS1 lies below I1 in the $C_7H + C_2H_2$ reaction, which is indicative of a negligible entrance barrier. I2 is unstable and can readily rearrange to a more stable intermediate *c*-$HC_{2n-1}(CH)CH$ (I4). Subsequently, I4 rearranges to the most-stable intermediate $HC_{2n+1}H_2$ (I6) either through hydrogen transfer followed by ring disclosure or *vice versa*. At exit channels, I4 decomposes to *c*-$^1HC_{2n-1}(C)CH$ + H and I6 decomposes to $^3HC_{2n+1}H$ + H and $^1H_2C_{2n+1}$ + H without any energy barrier. The product $^1H_2C_{2n+1}$ + H is energetically inaccessible in the present work. *c*-$^1HC_{2n-1}(C)CH$ and $^3HC_{2n+1}H_2$ are nearly isoenergetic with a difference less than 2 kcal mol^{-1}. Analogous to the *l*-$C_{2n-1}H$ (n = 2 – 4) + C_2H_2 reactions, we also found a vdW complex and a transition structure lying -1.3 and -0.7 kcal mol^{-1}, respectively, relative to the reactant at the entrance channel of the CH + C_2H_2 reaction. Furthermore, the reaction enthalpy for decomposition to *c*-$^1HC(C)CH$ (^3HCCCH) + H was calculated to be -24.0 (-12.6) kcal mol^{-1} that is in good agreement with the previous calculations.[36] Therefore, the CH + C_2H_2 reaction can be viewed as barrierless as the previous theoretical

calculations.[36]

c-$HC_{2n-3}(C)C$ (n = 2 – 4) can add to C_2H_2 through an energy barrier of height 5.5 – 7.4 kcal mol^{-1} (TS9 or TS10) to form a complex *c*-$HC_{2n-3}(C)CCHCH$ that has four conformers (I7, I8, I9 and I10) readily rearrange to one another through small energy barriers. The complex can decompose directly to *c*-$^1HC_{2n-3}(C)CCCH$ + H through a transition state TS15 or TS16, or isomerize to I4 that is the aforementioned cyclic intermediate of the *l*-$C_{2n-1}H$ + C_2H_2 reaction. Because the dissociation barrier (TS15 or TS16) is 12.2 – 13.5 kcal mol^{-1} above the isomerization barrier (TS17), the isomerization path is predicted to be more favorable. I4 in turn undergoes the mechanisms mentioned in the *l*-$C_{2n-1}H$ + C_2H_2 reaction. Since *l*-$C_{2n-1}H$ and *c*-$HC_{2n-3}(C)C$ have an energy difference less than 3 kcal mol^{-1} for n = 2 – 4 and their reactions appear to undergo the same mechanisms at exit channels, both the reactions cannot be distinguished in the present work. Nonetheless, the *c*-$HC_{2n-3}(C)C$ + C_2H_2 reaction is expected to be minor owing to the large entrance barrier.

The product translational energy extends to the energetic limit of the most-stable product isomer either *c*-$^1HC_{2n-1}(C)CH$ + H or $^3HC_{2n+1}H$ + H. The $C_{2n-1}H$ (n = 1 – 4) + C_2H_2 reactions have average translational-energy releases of 11.1, 4.7, 4.6, and 6.4 kcal mol^{-1} corresponding to fractions of 0.36, 0.38, 0.38, and 0.42, respectively, in translational degrees of freedom. Since a hydrogen atom carries no internal energy, the internal-energy distribution of product $C_{2n+1}H_2$ is derivable straightforward from the translational-energy distribution. After deconvolution from the photon-energy bandwidth ~ 0.42 eV, the ionization threshold was determined as 8.8 eV for C_3H_2, 8.5 eV for C_5H_2, 8.4 eV for C_7H_2, and 8.3 eV for C_9H_2 with an uncertainty of ± 0.2 eV. The adiabatic ionization energies of $^3HC_{2n+1}H$ and *c*-$^1HC_{2n-1}(C)CH$ were calculated as 8.62 and 9.12 eV for n = 1, 8.29 and 8.84 eV for n = 2, 7.94 and 8.61 eV for n = 3, and 7.69 and 8.49 eV for n = 4. The calculated value 9.12 eV of *c*-$^1HC(C)CH$ is in good agreement with the literature-reported experimental value 9.15 ± 0.03 eV,[40] indicating that the present theoretical calculation is reliable. The calculated adiabatic ionization energies of $^3HC_{2n+1}H$ and *c*-$^1HC_{2n-1}(C)CH$ are near the

deconvoluted ionization threshold. The combination of product's translational-energy distributions and photoionization spectra confirms the formation of *c*-$^1HC_{2n-1}(C)CH$ and/or $^3HC_{2n+1}H$. The quantum-chemical calculations indicate that the production to *c*-$^1HC_{2n-1}(C)CH$ + H is more straightforward than to $^3HC_{2n+1}H$ + H that needs ring disclosure and hydrogen transfer before decomposition. The asymptote $^1H_2C_{2n+1}$ (n = 2 – 4) + H is energetically inaccessible in the present work. We refrain from partitioning the $C_{2n+1}H_2$ product into both cyclic and linear isomers because of no prominent features for both product isomers on the translational-energy distributions and near the photoionization thresholds. The present experimental result on the reaction CH + C_2H_2 → C_3H_2 + H is in accord with the result of Maksyutenko et al.[29] without partitioning into linear and cyclic C_3H_2.

Kinematic constraints[41,42,43] can govern the angular-momentum disposal to some extent in a reaction system *A* + *BC* (***j***) → *AB* (***j'***) + *C*. ***j*** (***j'***) is reactant's (product's) rotational angular momentum, $\boldsymbol{\ell}$ ($\boldsymbol{\ell'}$) reactant's (product's) orbital angular momentum, and ***J*** the total angular momentum. $\boldsymbol{\ell}$ equals $\mu \times \boldsymbol{b} \times \mathbf{V}_{rel}$; μ is the reduced mass, ***b*** impact parameter, and $\mathbf{V}_{rel}$ relative velocity between two colliding reactants.[41] The five angular momenta obey the relation $\boldsymbol{j} + \boldsymbol{\ell} = \boldsymbol{J} = \boldsymbol{j'} + \boldsymbol{\ell'}$ that can be approximate to $\boldsymbol{\ell} \approx \boldsymbol{J} = \boldsymbol{j'} + \boldsymbol{\ell'}$ as $\boldsymbol{j} \approx 0$. On the basis of the kinematic model,[41,42,43] the angular-momentum disposal is expressible as $\boldsymbol{\ell'} = (\boldsymbol{\ell}–\boldsymbol{d})\times\cos^2\beta$. ***d*** is a dynamics-related angular momentum and $\cos^2\beta$ is a mass factor equal to $M_A \times M_C/(M_{BC} \times M_{AB})$. Regarding the title reaction as a triatomic system, $\cos^2\beta$ equals 0.013 for n = 1, 0.023 for n = 2, 0.027 for n = 3, and 0.030 for n = 4. Accordingly, ***J*** is deposited mostly to ***j'*** but minor to $\boldsymbol{\ell'}$. If $\boldsymbol{\ell'}$ is close to zero or its magnetic sublevels are equally populated, the product angular distribution will be nearly isotropic. Furthermore, the angular distribution will approach forward-backward symmetry as the ratio of lifetime to rotational period of the reaction complex or intermediate is much larger than unity.[44] Since the reactions of n = 2 – 4 are nearly isothermic in reaction enthalpy and have deep potential wells, the reaction complex or intermediate is expected to be

long-lived. Only the collision events that have ℓ values less than ℓ_{max} can overcome the centrifugal barrier at the entrance channel. Assuming the dispersion potential $V_{dis} = -C_6/R^6$ is dominant at the long range, the maximal angular momenta ℓ_{max} in the $C_{2n-1}H$ (n = 2 – 4) + C_2H_2 reactions are estimated as 213, 275, and 322 $\hbar$, respectively, based on the classical capture theory. The coefficient C_6 can be expressed in terms of ionization energies and isotropic polarizabilities of reactants.[45,46] The ℓ_{max} value corresponds to a rotational period 0.8, 1.9, and 3.5 (or 1.1, 2.3, and 4.0) ps of the intermediate I4 (or I6) about its principal axis *c* for n = 2 – 4.

Normalized to the same reactant ion signal, the type-2 reactions have a product-ion-signal ratio 1:0.13:0.07:0.25 for n = 1 – 4. Here, reactants $C_{2n-1}H$ were ionized with 12.5 eV and products $C_{2n+1}H_2$ were ionized with 11.6 eV. The four reactions have the same reactant collision velocity (V_{rel} = 2544 m s^{-1}) but different collision energies ($6.7 \le E_c \le 15.4$). The ion signals of each product were integrated in both the TOF distribution and the angular distribution. The nonreactive part was subtracted from the total ion signal based on the simulations shown in Figs. 3 and 4. Though this ratio cannot correlate straightforward to the relative reaction cross sections at the same E_c, the CH reaction appears to have a cross section greater than that of the C_3H, C_5H, and C_7H reactions for the hydrogen-loss channel. Because the reactants (products) belong to the family $C_{2n-1}H$ ($C_{2n+1}H_2$), their ionization cross sections and dissociative ionizations probably have similar functions of *n*. After normalization to the reactant ion signal, the effects of ionization cross sections and dissociative ionizations can be diminished or roughly cancelled on the product ion signal ratio. Regardless of the difference on reactant/product detection efficiency, the product ratio can be attributed to the following facts. First, the CH reaction is exothermic and barrierless but the C_3H and C_5H reactions are isoergic or slightly endothermic and have a small entrance barrier. The entrance barrier is below the reactant in the C_7H reaction, which might account for the slight enhancement on the product C_9H_2 compared with C_5H_2 and C_7H_2. Second, more exit channels open and become more competitive as the carbon number of $C_{2n-1}H$ increases from n = 1 to 4 and the corresponding collision energy increases from 6.7 to 15.4 kcal mol^{-1}. Besides, the

decomposition back to the reactant also becomes more significant as reactant collision energy increases. Third, the reactants $C_{2n-1}H$ (n = 2 – 4) possibly involve low-lying but less-reactive cyclic isomers in the radical beam. Though *c*-C_3H lies 1.4 kcal mol^{-1} below *l*-C_3H, the *c*-C_3H + C_2H_2 reaction has a barrier of height 7.4 kcal mol^{-1} at the entrance channel. Besides, *c*-$HC_3(C)C$ (*c*-$HC_5(C)C$) lies 2.9 (2.7) kcal mol^{-1} above *l*-C_5H (*l*-C_7H) but its reaction with C_2H_2 also has an entrance barrier of 6.8 – 7.0 (5.5 – 5.9) kcal mol^{-1}. Accordingly, the cyclic $C_{2n-1}H$ radical has reactivity less than its linear isomer in the present work.

In conjunction with the previous work on the reactions $C_{2n}H$ (n = 1 – 4) + $C_2H_2 \rightarrow C_{2n+2}H_2$ + H,[14] the reactions C_mH (m = 1 – 8) + $C_2H_2 \rightarrow C_{m+2}H_2$ + H have a product ion-signal ratio 0.36:1:0.05:0.30:0.03:0.18:0.09:0.23 as presented in Fig. 8. The $C_{2n-1}H$ + C_2H_2 reaction has a cross section less than the $C_{2n}H$ + C_2H_2 reaction for each *n* value, that is attributed to the difference on their potential-energy surfaces. *l*-$C_{2n-1}H$ can offer two unpaired electrons to bond with C_2H_2 for formation of either cyclic or linear complex that leads to a cyclic or linear $C_{2n+1}H_2$ product with a hydrogen atom. In contrast, *l*-$C_{2n}H$ offers only an unpaired electron to bond with C_2H_2 for formation of a linear complex that leads exclusively to a polyynic product with a hydrogen atom. The $C_{2n-1}H$/H exchange reaction is nearly isoergic but the $C_{2n}H$/H exchange reaction is quite exothermic so that the trajectory returning to the reactant asymptote in the former reaction is more significant than in the latter one. The CH/H exchange reaction is barrierless and exothermic so that it remains about one third of the cross section of the C_2H/H exchange reaction. In contrast to the barrierless reaction of $C_{2n}H$ + C_2H_2, the small entrance barrier in the $C_{2n-1}H$ + C_2H_2 reaction might reduce the b_{max} value and the reactive cross section estimated by the capture model. Because *c*-$C_{2n-1}H$ is less reactive than *l*-$C_{2n-1}H$, the abundance of *c*-$C_{2n-1}H$ in the radical beam diminishes the average reactivity of total $C_{2n-1}H$ species. The $C_{2n}H$ reactants were identified as *l*-$C_{2n}H$ exclusively by the PIE spectroscopy.

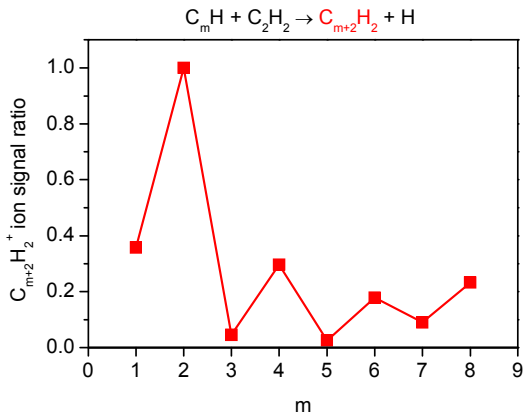

Figure 8. Relative ion-signal ratios of $C_{m+2}H_2$ produced from the reactions C_mH (m = 1 – 8) + C_2H_2 → $C_{m+2}H_2$ + H. The ion signal of C_4H_2 is set to unity.

Some concerns on the possible interferences from discharge side products to the crossed-beam reaction products $C_{2n+1}H_2$ are addressed here. First, the association of C_{2n-1} + C_2H_2 → $C_{2n+1}H_2$ was not observed in the present crossed-beam single-collision experiment. If the association takes place, the adduct $C_{2n+1}H_2$ should have a temporal distribution width and an angular distribution width less than the experimental observations. Second, the influence of the reaction $^{13}C^{12}C_{2n-2}$ + $^{12}C_2H_2$ (or $^{12}C_{2n-1}$ + $^{13}C^{12}CH_2$) → $^{13}C^{12}C_{2n}H$ + H to each title reaction was below 5% in the present work as mentioned in the section IV. Third, the discharge product $C_{2n-1}H_2$ (n = 2 – 5) has an interference on the detection of reaction product $C_{2n+1}H_2$ (n = 1 – 4), separately, by nonreactive scattering as presented in Figs. 3 and 4 but has no interference to $C_{2n+1}H_2$ through reactions with C_2H_2. Our theoretical calculations indicate that $C_{2n-1}H_2$ (n = 2 – 4) has two lowest-lying isomers *c*-$^1HC_{2n-3}(C)CH$ and $^3HC_{2n-1}H$; the latter lies 11.4, 1.9, and -1.3 kcal mol^{-1} relative to the former. Figure 9 indicates that the entrance barrier heights are 6.0, 9.4, 14.3, and 17.0 kcal mol^{-1} for the $^3HC_{2n-1}H$ (n = 1 – 4) + C_2H_2 reactions and 16.7, 16.0, and 15.6 kcal mol^{-1} for the *c*-$HC_{2n-3}(C)CH$ (n = 2 – 4) + C_2H_2 reactions. For the $^3CH_2$ + C_2H_2 reaction, the calculated

barrier height is in good agreement with the experimental activation energy 6.6 kcal mol^{-1}.[47] Furthermore, the decomposition to $C_{2n+1}H_3$ + H competes with to $C_{2n+1}H_2$ + H_2/2H. For instance, C_3H_3 rather than C_3H_2 was observed in the $^1CH_2$ + C_2H_2 reaction.[48] The TOF spectrum recorded at m/z = 12×(2×n+1)+3 has the same appearance as that recorded at 12×(2×n+1)+2 but the former signal is at least one order of magnitude less than the latter one. Therefore, the signal recorded at m/z = 12×(2×n+1)+3 is attributed to the ^{13}C isotopic variants and a mass leak of $C_{2n+1}H_2$. Fourth, the concentration ratio of reactants C_3H_2 to C_3H can be enhanced by a factor of 2.0 as the discharge medium is changed from 1% to 5% C_2H_2/He. It is found that the C_5H_2 product correlates strongly with the reactant C_3H rather than C_3H_2. Fifth, the species $C_{2n-1}H_y$ ($y \geq 3$) in the present radical beam is much less than $C_{2n-1}H$. Moreover, the $C_{2n-1}H_y$ ($y \geq 3$) + C_2H_2 reaction needs eject more than three hydrogen atoms to produce $C_{2n+1}H_2$ and thus cannot compete with the title reaction. Sixth, the interference of C_xH_y ($x > 2n-1$) + C_2H_2 reactions to the $C_{2n+1}H_2$ product by dissociative ionization was not observed with photon energy below 12 eV. If it occurs, the laboratory angular distribution of $C_{2n+1}H_2$ should peak at the Θ_{CM} of the C_xH_y + C_2H_2 reaction rather than of the $C_{2n-1}H$ + C_2H_2 reaction. Overall, the detected species $C_{2n+1}H_2$ is produced dominantly or exclusively from the title reaction that can account satisfactorily for the experimental results.

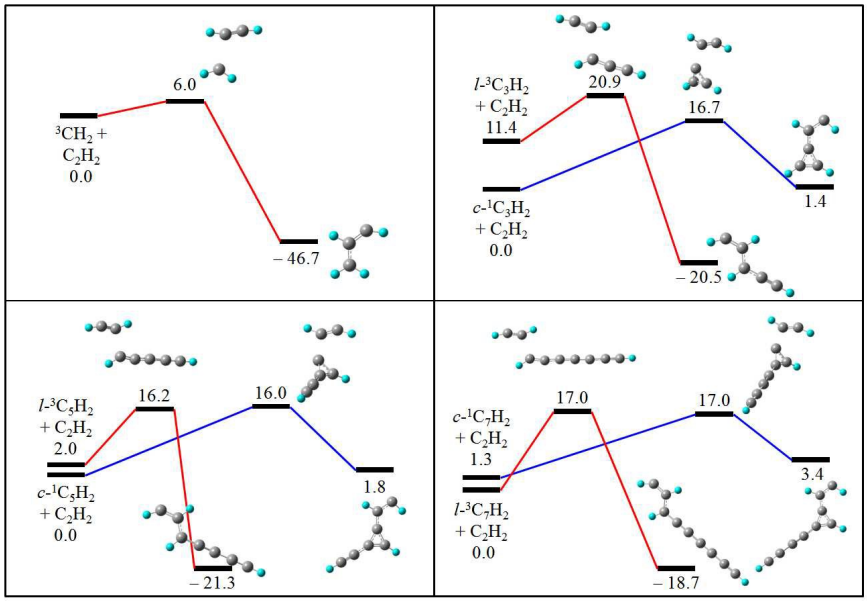

Figure 9. Potential-energy surfaces of the reactions $C_{2n-1}H_2$ (n = 1 – 4) + C_2H_2 → $C_{2n+1}H_4$. Red (blue) lines are for the linear (cyclic) $C_{2n-1}H_2$ reactions. The molecular structures are presented along with their potential-energy levels. The relative potential energies are given in kcal mol^{-1}.

Some implications for interstellar and combustion chemistry are given below. More than 20 molecular species including polyynes, methylpolyynes, cyanopolyynes, benzene, and other carbon-bearing species have been discovered in CRL 618.[49] The column densities of some hydrocarbon species were determined as $N(C_2H) = 2.0\times10^{15}$ cm^{-2}, $N(C_4H) = 1.2\times10^{15}$ cm^{-2}, $N(C_2H_2) = 2.0\times10^{17}$ cm^{-2}, $N(C_4H_2) = 1.2\times10^{17}$ cm^{-2}, and $N(C_6H_2) = 6.0\times10^{16}$ cm^{-2}.[7,50] The type-1 reactions are believed to play an important role for the formation of interstellar polyynes. The reaction C_2 + $C_{2n}H_2$ → $C_{2n+2}H$ + H is a source for the production of $C_{2n+2}H$. Due to the strong UV flux (~ 3×10^6 photons s^{-1}) from the central star,[51] photodissociation of polyynes is also a source for the production of $C_{2n+2}H$ in CRL 618. Atomic carbon is producible from CO by photolysis and is 0.7 times the column density 1×10^{19} cm^{-2} of CO.[52] Thus, the C + $C_{2n}H_2$ → $C_{2n+1}H$ + H reactions can initiate the synthesis of hydrocarbons with odd-numbered carbons. The column densities $N(l\text{-}C_3H)$

= 8.3×10^{14} cm^{-2}, N(c-C_3H) = 2.5×10^{15} cm^{-2}, N(c-C_3H_2) = 1.8×10^{16} cm^{-2}, and N(C_5H) = 2.5×10^{14} cm^{-2} are derivable from the reported abundance ratios with respect to HC_3N;[15] here, N(HC_3N) = 5.0×10^{16} cm^{-2} (Ref. 53) is employed as the reference. A chemical model[49] also predicted that $C_{2n+1}H$ and $C_{2n+1}H_2$ (n = 1 – 3) have column densities ~ 10^{15} cm^{-2} in CRL 618. Therefore, we suggest that the reactions CH + $C_{2n}H_2$ → $C_{2n+1}H_2$ + H and $C_{2n-1}H$ + C_2H_2 → $C_{2n+1}H_2$ + H can take place in CRL 618 where the temperature is 250 – 800 K.[54]

Because of the existence of $C_{2n-1}H$ (n = 1 – 4) in IRC+10216[5] and in TMC-1,[3,4,16,17] $C_{2n+1}H_2$ is expected to be formed from the type-2 reaction in these two interstellar media. Up to date, however, only l-H_2C_3 (propadienylidene) and c-C_3H_2 (cyclopropenylidene) are discovered in the dense molecular cloud TMC-1[3] and the circumstellar envelope of IRC+10216[5] where the temperatures are ~ 10 K and ~ 25 K, respectively. The RRKM calculations predicted that the branching ratio was 84.5–87.0% for $^3HC_3H$ + H, 10.2–12.8% for c-C_3H_2 + H, 0.9% for H_2C_3 + H, and the rest for C_3H + H_2 in the CH + C_2H_2 reaction at E_c = 0 kcal mol^{-1}.[36] Accordingly, $^3HC_3H$ might be the most-probable candidate to be discovered in these two interstellar media. The entrance barrier height and/or the reaction endothermicity, albeit small based on the present calculations, might hinder the proceeding of the $C_{2n-1}H$ (n = 2 – 4) + C_2H_2 reactions in extremely cold interstellar space. It is possible to produce $C_{2n+1}H_2$ from the reactions (2) in the inner circumstellar shell of IRC+10216 where the temperature and gas density are sufficiently high.

In fuel-rich flames of several hydrocarbons, C_2H_2, C_3H_2, C_4H_2, C_5H_2, C_6H_2, C_8H_2, and $C_{10}H_2$ could be detected using flame-sampling molecular-beam synchrotron-photoionization mass spectrometry[8,18,19,20,21] but $C_{2n-1}H$ and $C_{2n}H$ radicals remained elusive due to their high reactivities and low concentrations. The reactions in eq. (1) are believed to play an important role in the syntheses of polyynes ($HC_{2n+2}H$). In contrast to the closed-shell polyynes, the $C_{2n+1}H_2$ radicals are more reactive with combustion fuels and intermediates. Thus, $C_{2n+1}H_2$ (n ≥ 3) is hard to be accumulated to a high concentration level for detection even though in a fuel-rich flame. In addition to the type-1 reactions, the type-2 reactions need also be taken into account in combustion

chemistry models in order to give a whole picture for the series of reactions C_mH ($m \geq 1$) + C_2H_2 → $C_{m+2}H_2$ + H in a flame.

VI. Conclusions

The dynamics of reactions $C_{2n-1}H$ (n = 1 – 4) + C_2H_2 → $C_{2n+1}H_2$ + H were explored in crossed molecular beams using product translational and photoionization spectroscopy. The *l*-$C_{2n-1}H$ radical adds to the triple bond of C_2H_2 to form a cyclic complex *c*-$HC_{2n-1}(CH)CH$ (I4) that either decomposes directly to *c*-$^1HC_{2n-1}(C)CH$ + H or rearranges to $HC_{2n+1}H_2$ (I6) followed by decomposition to $^3HC_{2n+1}H$ + H. The CH reaction is exoergic but the C_3H, C_5H, and C_7H reactions are nearly isoergic or slightly endothermic for the two hydrogen-loss channels. The translational-energy release extends to the energetic limit of product *c*-$^1HC_{2n-1}(C)CH$ + H or $^3HC_{2n+1}H$ + H. The kinematic model can qualitatively interpret the less anisotropic angular distributions of the hydrogen-loss channels. The combination of product translational-energy distributions and photoionization spectra suggests the productions of *c*-$^1HC_{2n-1}(C)CH$ and/or $^3HC_{2n+1}H$, though both the isomers cannot be well resolved in the present work. Further experimental and theoretical investigations are required in order to obtain the ratios branching to these two exit channels. The present work suggests that the title reactions, notably the CH + C_2H_2 reaction, can take place in warmer or hotter interstellar/circumstellar environments and in combustion processes. In conjunction with the previous work on the reactions $C_{2n}H$ (n = 1 – 4) + C_2H_2 → $C_{2n+2}H_2$ + H, a brief picture for the reactions C_mH (m = 1 – 8) + C_2H_2 → $C_{m+2}H_2$ + H can be outlined. The $C_{2n-1}H$/H exchange reaction has a cross section less than the $C_{2n}H$/H exchange reaction for each *n* value ranging from 1 to 4. The differences between both types of reactions (1) and (2) are stated.

Acknowledgements

We thank the National Synchrotron Radiation Research Center (NSRRC) and the Ministry of

Science and Technology (MOST) of Taiwan (Grant No. MOST103-2113-M-213-003-MY3) for financial supports.

References

1 P. Pratap, J. E. Dickens, R. L. Snell, M. P. Miralles, E. A. Bergin, W. M. Irvine and F. P. Schloerb, *Astrophys. J.*, 1997, **486**, 862–885.

2 M. Guelin, P. Friberg and A. Mezaoui, *Astron. Astrophys.*, 1982, **109**, 23–31.

3 D. Fosse, J. Cernicharo, M. Gerin and P. Cox, *Astrophys. J.*, 2001, **552**, 168–174.

4 J. E. Dickens, W. D. Langer and T. Velusamy, *Astrophys. J.*, 2001, **558**, 693–701.

5 L. M. Ziurys, *Proc. Natl. Acad. Sci. U. S. A.*, 2006, **103**, 12274–12279.

6 N. A. Teanby, P. G. J. Irwin, R. de Kok, A. Jolly, B. Bezard, C. A. Nixon and S. B. Calcutt, *Icarus*, 2009, **202**, 620–631.

7 J. Cernicharo, A. M. Heras, A. G. G. M. Tielens, J. R. Pardo, F. Herpin, M. Guelin and L. B. F. M. Waters, *Astrophys. J.*, 2001, **546**, L123–L126.

8 N. Hansen, S. J. Klippenstein, P. R. Westmoreland, T. Kasper, K. Kohse-Hoinghaus, J. Wang and T. A. Cool, *Phys. Chem. Chem. Phys.*, 2008, **10**, 366–374.

9 D. Chastaing, P. L. James, I. R. Sims and I. W. M. Smith, *Faraday Discuss.*, 1998, **109**, 165–181.

10 A. B. Vakhtin, D. E. Heard, I. W. M. Smith and S. R. Leone, *Chem. Phys. Lett.*, 2001, **344**, 317–324.

11 C. Berteloite, S. D. Le Picard, P. Birza, M.-C. Gazeau, A. Canosa, Y. Benilan and I. R. Sims, *Icarus*, 2008, **194**, 746–757.

12 C. Berteloite, S. D. Le Picard, N. Balucani, A. Canosa and I. R. Sims, *Phys. Chem. Chem. Phys.*, 2010, **12**, 3677–3689.

13 R. I. Kaiser, F. Stahl, P. v. R. Schleyer and H. F. Schaefer III, *Phys. Chem. Chem. Phys.*, 2002, **4**, 2950–2958.

14 Y.-L. Sun, W.-J. Huang and S.-H. Lee, *J. Phys. Chem. Lett.*, 2015, **6**, 4117–4122. (DOI: 10.1021/acs.jpclett.5b01910).

15 J. R. Pardo and J. Cernicharo, *Astrophys. J.*, 2007, **654**, 978–987.

16 A. Suutarinen, W. D. Geppert, J. Harju, A. Heikkila, S. Hotzel, M. Juvela, T. J. Millar, C. Walsh and J. G. A. Wouterloot, *Astron. Astrophys.*, 2001, **531**, A121.

17 M. Ohishi and N. Kaifu, *Faraday Discuss*., 1998, **109**, 205–216.

18 P. R. Westmoreland, J. B. Howard and J. P. Longwell, *Proc. Combust. Inst.*, 1986, **21**, 773.

19 A. Bhargava and P. R. Westmoreland, *Combust. Flame*, 1998, **113**, 333–347.

20 S. D. Thomas, A. Bhargava, P. R. Westmoreland, R. P. Lindstedt and G. Skevis, *Bull. Soc. Chim. Belg.*, 1996, **105**, 501–512.

21 C. A. Taatjes, S. J. Klippenstein, N. Hansen, J. A. Miller, T. A. Cool, J. Wang, M. E. Law and P. R. Westmoreland, *Phys. Chem. Chem. Phys.*, 2005, **7**, 806–813.

22 N. Hansen, S. J. Klippenstein, J. A. Miller, J. Wang, T. A. Cool, M. E. Law, P. R. Westmoreland, T. Kasper and K. Kohse-Hoinghaus, *Phys. Chem. Chem. Phys.*, 2006, **110**, 4376–4388.

23 A. Canosa, I. R. Sims, D. Travers, I. W. M. Smith and B. R. Rowe, *Astron. Astrophys.*, 1997, **323**, 644–651.

24 J. E. Butler, J. W. Fleming, L. P. Goss and M. C. Lin, *Phys. Chem. Chem. Phys.*, 1981, **56**, 355–365.

25 M. R. Berman, J. W. Fleming, A. B. Harvey and M. C. Lin, *Chem. Phys.*, 1982, **73**, 27.

26 H. Thiesemann, J. MacNamara and C. A. Taatjes, *J. Phys. Chem. A*, 1997, **101**, 1881.

27 J. C. Loison and A. Bergeat, *Phys. Chem. Chem. Phys.*, 2009, **11**, 655–664.

28 K. McKee, M. A. Blitz, K. J. Hughes, M. J. Pilling, H.-B. Qian, A. Taylor and P. W. Seakins, *J. Phys. Chem. A*, 2003, **107**, 5710–5716.

29 P. Maksyutenko, F. Zhang, X. Gu and R. I. Kaiser, *Phys. Chem. Chem. Phys.*, 2011, **13**, 240–252.

30 R. I. Kaiser, X. Gu, F. Zhang and P. Maksyutenko, *Phys. Chem. Chem. Phys.*, 2012, **14**, 575–588.

31 W. Boullart, K. Devriendt, R. Borms and J. Peeters, *J. Phys. Chem.*, 1996, **100**, 998–1007.

32 F. Goulay, A. J. Trevitt, G. Meloni, T. M. Selby, D. L. Osborn, C. A. Taatjes, L. Vereecken and S. R. Leone, *J. Am. Chem. Soc.*, 2009, **131**, 993–1005.

33 R. Guadagnini, G. C. Schatz and S. P. Walch, *J. Phys. Chem. A*, 1998, **102**, 5857–5866.

34 L. Vereecken, K. Pierloot and J. Peeters, *J. Chem. Phys.*, 1998, **108**, 1068–1080.

35 L. Vereecken and J. Peeters, *J. Phys. Chem. A*, 1999, **103**, 5523–5533.

36 T. L. Nguyen, A. M. Mebel, S. H. Lin and R. I. Kaiser, *J. Phys. Chem. A*, 2001, **105**, 11549–11559.

37 S.-H. Lee, W.-K. Chen and W.-J. Huang, *J. Chem. Phys.*, 2009, **130**, 054301.

38 I-C. Lu, W.-J. Huang, C. Chaudhuri, W.-K. Chen and S.-H. Lee, *Rev. Sci. Instrum.*, 2007, **78**, 083103.

39 W.-J. Huang, Y.-L. Sun, C.-H. Chin and S.-H. Lee, *J. Chem. Phys.*, 2014, **141**, 124314.

40 H. Clauberg, D. W. Minsek and P. Chen, *J. Am. Chem. Soc.*, 1992, **114**, 99–107.

41 R. D. Levine, *Molecular Reactive Dynamics*, Cambridge Univ. Press, New York, 2005.

42 I. R. Elsum and R. G. Gordon, *J. Chem. Phys.*, 1982, **76**, 3009–3018.

43 I. Schechter, R. D. Levine and R. G. Gordon, *J. Phys. Chem.*, 1991, **95**, 8201–8205.

44 W. B. Miller, S. A. Safron and D. R. Herschbach, *Discuss. Faraday Soc.*, 1967, **44**, 108–122.

45 J. O. Hirschfelder, C. F. Curtiss and R. B. Bird, *Molecular Theory of Gases and Liquids*, Wiley, New York, 1954.

46 S.-H. Lee, W.-K. Chen, C.-H. Chin and W.-J. Huang, *J. Chem. Phys.*, 2013, **139**, 064311.

47 D. L. Baulch, C. J. Cobos, R. A. Cox, C. Esser, P. Frank, Th. Just, J. A. Kerr, M. J. Pilling, J. Troe, R. W. Walker and J. Warnatz, *J. Phys. Chem. Ref. Data*, 1992, **21**, 411–429.

48 H. F. Davis, J. Shu, D. S. Peterka and M. Ahmed, *J. Chem. Phys.*, 2004, **121**, 6254–6257.

49 P. M. Woods, T. J. Millar, E. Herbst and A. A. Zijlstra, *Astron. Astrophys.*, 2003, **402**, 189–199.

50 S. Fukasaku, Y. Hirahara, A. Masuda, K. Kawaguchi, S. Ishikawa, N. Kaifu and W. M. Irvine, *Astrophys. J.*, 1994, **437**, 410–418.

51 A. J. Remijan, F. Wyrowski, D. N. Friedei, D. S. Meier and L. E. Snyder, *Astrophys. J.*, 2005, **626**, 233–244.

52 K. Young, *Astrophys. J.*, 1997, **488**, L157–L160.

53 J. Cernicharo, A. M. Heras, J. R. Pardo, A. G. G. M. Tielens, M. Guelin, E. Dartois, R. Neri and L. B. F. M. Waters, *Astrophys. J.*, 2001, **546**, L127–L130.

54 F. Herpin and J. Cernicharo, *Astrophys. J.*, 2000, **530**, L129–L132.